

SCIENTIFIC REPORTS



OPEN

Wide-angle Spectrally Selective Perfect Absorber by Utilizing Dispersionless Tamm Plasmon Polaritons

Received: 26 August 2016
Accepted: 22 November 2016
Published: 19 December 2016

Chun-hua Xue^{1,2}, Feng Wu², Hai-tao Jiang², Yunhui Li², Ye-wen Zhang² & Hong Chen²

We theoretically investigate wide-angle spectrally selective absorber by utilizing dispersionless Tamm plasmon polaritons (TPPs) under TM polarization. TPPs are resonant tunneling effects occurring on the interface between one-dimensional photonic crystals (1DPCs) and metal slab, and their dispersion properties are essentially determined by that of 1DPCs. Our investigations show that dispersionless TPPs can be excited in 1DPCs containing hyperbolic metamaterials (HMMs) on metal substrate. Based on dispersionless TPPs, electromagnetic waves penetrate into metal substrate and are absorbed entirely by lossy metal, exhibiting a narrow-band and wide-angle perfect absorption for TM polarization. Our results exhibit nearly perfect absorption with a value over 98% in the angle of incidence region of 0–80 degree.

Metamaterials are artificial microstructures that exhibit unusual optical properties beyond those available in nature. Appropriately designed metamaterials can be used for engineering electromagnetic (EM) space and controlling the propagation of EM waves, which exhibit many novel phenomena and promote many applications including negative refraction¹, perfect lenses², cloaking devices³ and so on. Recently, another important application, spectrally selective perfect absorbers⁴ have received considerable attention due to their importance for developing sensitive detectors for security related applications⁵ as well as narrow-band thermal emitters for thermophotovoltaic applications^{6–8}. In addition to narrow-band response, wide-angle response also is important for spectrally selective absorption since angular directivity of absorption essentially broadens the emission spectrum and thus is detrimental for these applications. Metamaterials including metasurfaces possess the abilities of confining EM fields and engineering photonic dispersion, which can be used for realizing wide-angle spectrally selective absorption. Physically speaking, the excitation of dispersionless optical resonance in the structure with blocked transmission (metal screening or the total reflection regime) can lead to wide-angle optical absorption. On the basis of this mechanism, researchers have realized wide-angle optical absorption in nanostructured metal surfaces⁹ and periodically patterned graphene¹⁰. Other absorptive microstructures for realizing wide-angle optical absorption include nanodisks^{11,12}, nanorods¹³, grating¹⁴ as well as other metallic patterns^{15,16}.

Based on the excitation of dispersionless Tamm plasmon polaritons, in this paper we explore the possibilities of realizing a wide-angle spectrally selective perfect absorber in a *simple* multilayer structure. The multilayer structure what we consider is a one-dimensional photonic crystal (1DPC) containing hyperbolic metamaterials (HMMs) on a metal substrate. It is well known that an EM surface state (so-called Tamm plasmon polariton, TPP) exists on the interface between 1DPC and metal substrate for frequencies within photonic band gap^{17,18}. At resonance frequency, there is a buildup of energy on the interface which depends on coupling of evanescent waves, giving up to resonant tunneling effect without reflection. By utilizing the unique properties of resonant tunneling effect, TPPs have exhibited a variety of applications such as optical switching and diode^{19,20}, second and third harmonic generation enhancement^{21,22}, lasing²³ as well as single photon emission²⁴. Undoubtedly, the properties of TPPs also can be used for narrow-band perfect absorption.

It is noteworthy that conventional TPPs are always dispersive owing to the angle-dependent properties of photonic band gap^{17,18}. For obtaining angle-insensitive TPPs, an angle-independent band gap is highly desirable.

¹School of Computer Science & Communication Engineering, Guangxi University of Science and Technology, Liuzhou, Guangxi 545006, China. ²Key Laboratory of Advanced Micro-structure Materials, MOE, School of Physics Science and Engineering, Tongji University, Shanghai 200092, China. Correspondence and requests for materials should be addressed to C.H.-X. (email: davies2000@163.com)

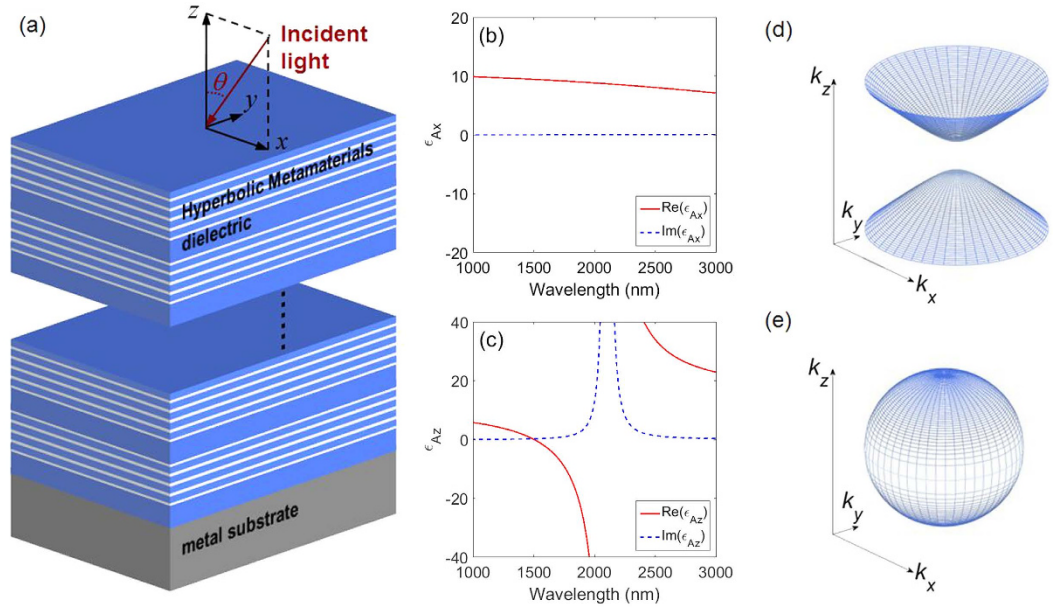


Figure 1. (a) The scheme of multilayer structure $((CD)_S)_N$ on a metal substrate. Here HMM layer is mimicked by a subwavelength metallodielectric stack $(CD)_S$. TM-polarized EM wave launches into the structure in $x-z$ plane with angle of incidence θ . (b) The effective permittivity tensor ϵ_{Ax} and (c) ϵ_{Az} of substructure $(CD)_S$. Layer C is Si with $d_C = 39\text{ nm}$ and Layer D is ITO with $d_D = 11\text{ nm}$. In the wavelength region of $1503\text{--}2103\text{ nm}$ substructure $(CD)_S$ can be mimicked as type-I HMMs. (d) Isofrequency surface in dispersion relation $k_x^2/\epsilon_x + k_z^2/\epsilon_z = k_0^2$ for type-I HMMs with $\epsilon_x > 0$ and $\epsilon_z < 0$, which indicates $\partial k_z/\partial k_x > 0$. By contrast, isofrequency surface for conventional isotropic medium with $\epsilon_x = \epsilon_z > 0$ is exhibited in (e), which indicates $\partial k_z/\partial k_x < 0$.

Very recently, our investigations show the existence of a dispersionless band gap in 1DPC containing HMMs²⁵. HMMs are highly anisotropic mediums with hyperbolic dispersion^{26–28} in which one of the principal components of their permittivity (permeability) tensors is opposite in sign to the other two principal components. Since it supports propagating modes with very large wave vectors, HMMs bring about a rich variety of new physics and novel applications such as sub-diffraction imaging²⁹, sub-wavelength modes³⁰, and spontaneous^{31–35} and thermal emission engineering^{36–38}. Moreover, in near-infrared or visible region, HMMs can be mimicked by a 1D metal-dielectric stack with subwavelength unit cell^{39–41}, which provides a convenient method for experimental implementation of HMMs. It should be pointed out that HMMs not only support high- k waves but also possess anomalous wavevector dispersion by contrast with isotropic dielectric. Anomalous wavevector dispersion in HMMs can compensate normal wavevector dispersion in isotropic dielectric. Such effect, so-called *phase variation compensation effect*, can be used for realizing dispersionless gap in 1DPCs containing HMMs²⁵. Since dispersion properties of TPPs depend on that of band gap of 1DPC, we can expect that TPP mode appearing on 1DPC-metal interface will be a dispersionless one. As a result, at resonant wavelength, EM wave penetrating into lossy metal slab and is absorbed entirely. Our results exhibit excellent performance of the structure with a nearly perfect wide-angle absorption with values over 98% in infrared region.

Structure and Parameters

As is shown in Fig. 1, the multilayer structure proposed is a 1DPC containing HMMs on a metal substrate, which is denoted by $((CD)_S)_N$. The structure $(CD)_S$ is a subwavelength metal-dielectric stack with thickness d_C of layer C, thickness d_D of layer D and period number S . Thickness $d_C + d_D$ of unit cell is much smaller than wavelength of EM wave within the structure, in the condition of long wavelength limit. Thus the effective-medium approach is valid so that substructure $(CD)_S$ can mimic a HMM layer with thickness $d_A = S(d_C + d_D)$ in proper frequency region. Then alternate layers of substructure $(CD)_S$ and dielectric B constitute 1DPC $((CD)_S)_N$ with period number N . The metal substrate is silver and its permittivity ϵ_M is referred to ref. 42. The input media are air. Moreover, we consider that electromagnetic waves with transverse-magnetic (TM) polarization launch into the structure in $x-z$ plane with angle of incidence θ . The magnetic field is in the y direction.

In the structure, dielectric B and C are selected to be Si with refractive index $n_{Si} = 3.48$ (i.e. permittivity $\epsilon_{Si} = n_{Si}^2 = 12.11$)⁴². Material D is selected to be indium-tin-oxide (ITO). ITO is a good candidate as plasmonic materials in infrared and visible region⁴³. The permittivity of ITO is described by a Drude-Lorentz model⁴⁴

$$\epsilon_D(\omega) = \epsilon'_\infty + \frac{(\epsilon_s - \epsilon'_\infty)\omega_{ID}^2}{\omega_{ID}^2 - \omega^2 - i\gamma'_D\omega} - \frac{\omega_{pD}^2}{\omega^2 + i\gamma_D\omega}, \quad (1)$$

where $\epsilon'_\infty = 0.04$ represents the high-frequency dielectric constant, $\epsilon_s = 3.48$ the strength of Lorentz oscillator, $\omega_{LD} = 2\pi \times 1640 \text{ THz}$ the frequency of Lorentz oscillator, $\gamma'_D = 0.038 \omega_{LD}$ the damping factor of Lorentz oscillator, $\omega_{pD} = 2\pi \times 375 \text{ THz}$ the plasma frequency, and $\gamma_{pD} = 0.00645 \omega_{pD}$ the damping constant.

With respect to structural parameters, we consider $d_C = 39 \text{ nm}$, $d_D = 11 \text{ nm}$, $d_B = 66 \text{ nm}$, $S = 5$ and $N = 13$. For substructure $(CD)_S$, its thickness of unit cell is $d_C + d_D = 50 \text{ nm}$, which exhibits subwavelength scale in the infrared range, and thus effective-medium approach is available for substructure $(CD)_S$. According to effective-medium approach, substructure $(CD)_S$ can be equivalent to a homogeneous medium A and its components of effective permittivity tensor for TM polarization are given by^{27,28}

$$\begin{aligned} \epsilon_{Ax} &= \epsilon_C(1 - p) + \epsilon_D p \\ \epsilon_{Az} &= \frac{1}{\frac{1-p}{\epsilon_C} + \frac{p}{\epsilon_D}}, \end{aligned} \quad (2)$$

where filling ratio $p = d_D / (d_C + d_D)$ is the volume percentage of layer D in unit cell of substructure. The effective permittivity tensors of substructure $(CD)_S$ are shown in Fig. 1(b) and (c). It can be seen that the effective permittivity tensors $\text{Re}(\epsilon_{Ax}) > 0$ and $\text{Re}(\epsilon_{Az}) < 0$ in the wavelength region of $1503 \sim 2103 \text{ nm}$, which corresponds to type-I HMMs.

The anomalous wavevector dispersion of HMM provides a specific method for engineering the dispersion of photonic band gap. Figure 1(d) and (e) exhibit isofrequency surfaces of type-I HMMs and isotropic dielectric, respectively. Isofrequency surface of type-I HMMs and isotropic dielectric are given by $k_x^2 / \epsilon_{Az} + k_{Az}^2 / \epsilon_{Ax} = k_0^2$ and $k_x^2 + k_{Bz}^2 = \epsilon_B k_0^2$, respectively, where k_{Az} and k_{Bz} are the z components of wavevector of substructure $(CD)_S$ and dielectric material B, respectively. $k_x = k_0 \sin \theta$ is the x component of wavevector, and $k_0 = \omega / c$ is wavevector in vacuum with ω being angular frequency and c being the speed of light. We can find that $\partial k_{Az} / \partial k_x > 0$ for type-I HMMs and $\partial k_{Bz} / \partial k_x < 0$ for conventional dielectric material. It means that k_{Az} will increase with the increase of θ but k_{Bz} will decrease with the increase of θ . As a result, HMMs exhibit anomalous wavevector dispersion by contrast with isotropic dielectric. Therefore, when alternate substructure $(CD)_S$ and dielectric layer B constitutes 1DPC $((CD)_S B)_N$, the increase of k_{Az} in substructure $(CD)_S$ can compensate the decrease of k_{Bz} in dielectric layer B. Such effect, so-called *phase variation compensation effect*, can be evolved as follows²⁵

$$\left(d_A \frac{\partial k_{Az}}{\partial k_x} + d_B \frac{\partial k_{Bz}}{\partial k_x} \right) \Bigg|_{\lambda_{\text{BrG}}} = 0. \quad (3)$$

Equation (3) can be used for designing the parameters of 1DPC $((CD)_S B)_N$ with dispersionless gap. In fact, for the parameters of 1DPC $((CD)_S B)_N$ in this work, a dispersionless gap with angle-independent Bragg wavelength λ_{BrG} can be realized on the basis of phase variation compensation effect. In context, we will illustrate its reflection properties in detail.

Results and Discussion

In the heterostructure composed of 1DPC and metal substrate, it is known that TPPs can exist on 1DPC-metal interface^{17,18}. For obtaining phase matching condition of TPPs, we assume there is a virtual air layer with thickness d_0 located between 1DPC and metal substrate. Then we use $\phi_0 = (d_0 \omega / c) \cos \theta$ to denote the phase shift of a propagating wave in the virtual air layer, and ϕ_M and ϕ_{PC} to denote the reflection phases of a propagating wave along z axis upon the metal from the virtual air layer and that upon the 1DPC from the virtual air layer, respectively. With these definitions, the resonance condition of eigenmode of the structure can be written as^{17,18}

$$\phi_M + \phi_{PC} + \phi_0 = 2m\pi, \quad (4)$$

where m is zero or an integer. If the length of the virtual air layer d_0 is set to zero and the values of ϕ_M and ϕ_{PC} are restricted in the interval of $(-\pi, \pi)$, Eq. (4) can be rewritten as the form

$$\phi_M + \phi_{PC} = 0. \quad (5)$$

Equation (5) represents phase matching condition of TPPs. The reflection coefficients r_M on metal substrate for a TM-polarized wave is given by the usual Fresnel formula

$$r_M = \frac{\sqrt{\epsilon_M - \sin^2 \theta} - \epsilon_M \cos \theta}{\sqrt{\epsilon_M - \sin^2 \theta} + \epsilon_M \cos \theta}. \quad (6)$$

Since in infrared regime the real part of permittivity of metal is the order of -10^2 and its imaginary part is about 10% of its real part, we assume $\epsilon_M = \epsilon'_M + i\epsilon''_M = -|\epsilon_M| \exp(-i\delta)$ with δ being the loss angle. Moreover, we do not consider the case of large angle of incidence so as to avoid $\cos \theta \rightarrow 0$. Under these conditions, Eq. (6) can be further derived with the first order Taylor approximation as

$$r_M \approx -1 + \frac{2\sqrt{\epsilon_M}}{\epsilon_M \cos \theta} \approx \left(-1 + \frac{2 \sin \frac{\delta}{2}}{\sqrt{|\epsilon_M|} \cos \theta} \right) \left[1 + i \frac{2}{\sqrt{|\epsilon_M|} \cos \theta} \right]. \quad (7)$$

Therefore the reflection phase upon metal substrate yields to

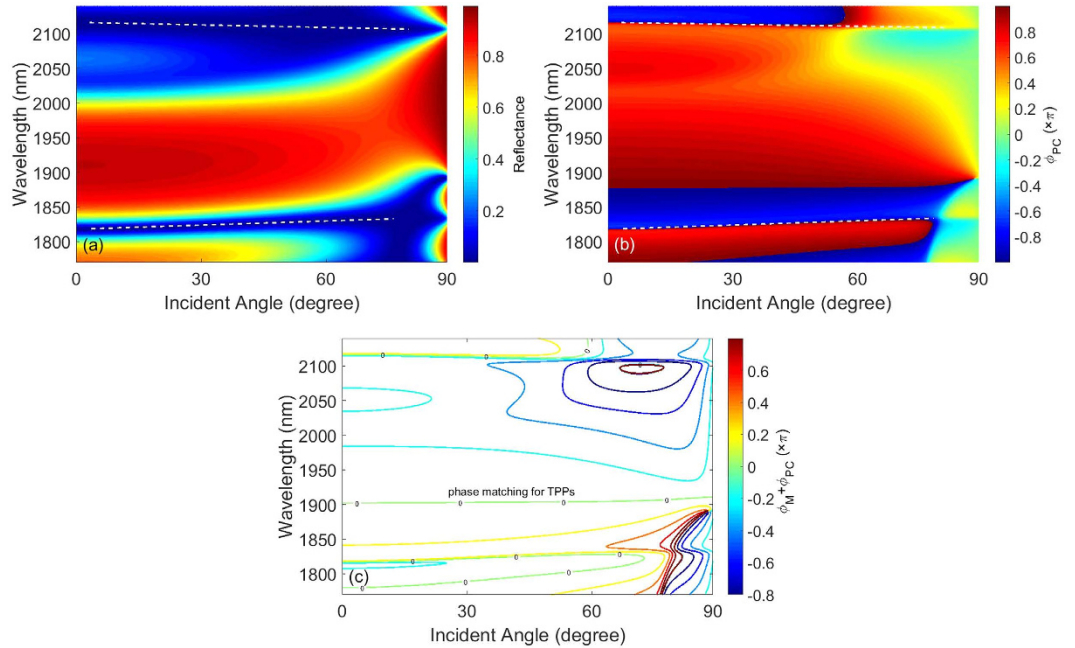


Figure 2. (a) The reflectance spectrum and (b) reflectance phase upon 1DPC $((CD)_S B)_N$, respectively. The area surrounded by white dashed line indicates band gap. (c) The contour of sum of reflection phases $\phi_M + \phi_{PC}$. Phase matching condition is satisfied at 1902 nm for all angles of incidence.

$$\phi_M = -\pi + \arctan\left(\frac{2}{\sqrt{|\varepsilon_M|} \cos\theta}\right) \approx -\pi + \frac{2}{\sqrt{|\varepsilon_M|} \cos\theta}. \quad (8)$$

The imaginary part of permittivity of silver will influence the reflection amplitude upon metal substrate but not the reflection phase. Besides, as $|\varepsilon_M| \gg 1$, the shift of ϕ_M with respect to optical wavelength is very weak. Return to Eq. (5) and we can find that the dispersion properties of TPPs are essentially determined by that of 1DPCs. It means that we require an angle-insensitive band gap structure to be used for realizing angle-independent TPPs.

1DPC containing HMMs provides opportunities for realizing angle-independent TPPs. Using transfer matrix method, the reflectance spectrum and reflection phase shift of a propagating wave along $-z$ axis upon 1DPC $((CD)_S B)_N$ are given in Fig. 2(a) and (b), respectively. For normal incidence, the reflectance of 1DPC reaches the minimum at 2117 nm and 1818 nm, respectively, which indicates the edges of band gap. Here wavelength 2117 nm corresponds to the lower band edge and 1818 nm corresponds to the upper one. Moreover, for oblique incidence, as is shown by white dashed lines in Fig. 2(a), the shift of band edges is very weak with an increase of angle of incidence. The results show that the shift of lower band edge just is 11 nm and that of upper band edge just is 16 nm, which is much smaller than corresponding optical wavelength. In Fig. 2(b), we also find that the reflection phase ϕ_{PC} of 1DPC $((CD)_S B)_N$ shifts from π at the lower band edge to $-\pi$ at the upper band edge. It is noteworthy that, in the wavelength region from 1878 nm to 2117 nm, the reflection phase ϕ_{PC} shifts in the interval of $[0, \pi]$. Particularly in the vicinity of 1878 nm, ϕ_{PC} is close to π . In such a wavelength, the reflection of 1DPC is analogous with that of magnetic negative materials. It is known that the resonant tunneling effect occurs when 1DPC within band gap exhibits magnetic negative properties⁴⁵. Therefore we can predict that the resonant tunneling effect occurs in the vicinity of 1878 nm. More importantly, for oblique incidence, the shift of ϕ_{PC} is rather weak with respect to angle of incidence in such a wavelength. Consequently, the resonant tunneling effect occurring in the vicinity of 1878 nm will be insensitive to angle of incidence. In fact, as is shown in Fig. 2(c), the sum of $\phi_M + \phi_{PC}$ is zero in the vicinity of 1902 nm for all angles of incidence, which exhibits wide-angle phase matching for TPP mode.

When 1DPC is combined with metal substrate, TPPs exciting on 1DPC-metal interface give rise to strong light absorption. Using transfer matrix method, the absorption spectra of the structure are illustrated in Fig. 3(a). Intuitively, a flat and near-perfect absorption band appears in the vicinity of 1902 nm. Essentially, this near-perfect absorption band is resulted from TPPs existing on 1DPC-metal interface. As a typical example, we calculate the magnetic field distributions at 1902 nm for normal incidence in Fig. 3(b). It can be found that the Bloch wave in 1DPC along z axis is magnified exponentially and finally is localized on 1DPC-metal interface. The incident EM waves hence penetrate into metal substrate and are absorbed entirely by lossy metal. It should be pointed out that the narrow-band and wide-angle absorption is polarization-dependent. If we change TM polarization to TE, the wavevector dispersion of HMM is similar to an isotropic medium, and hence TPPs in the structure for TE polarization is dispersive which is similar to conventional TPPs. As a result, the narrow-band and wide-angle absorption can be obtained only for TM polarization but not for TE polarization.

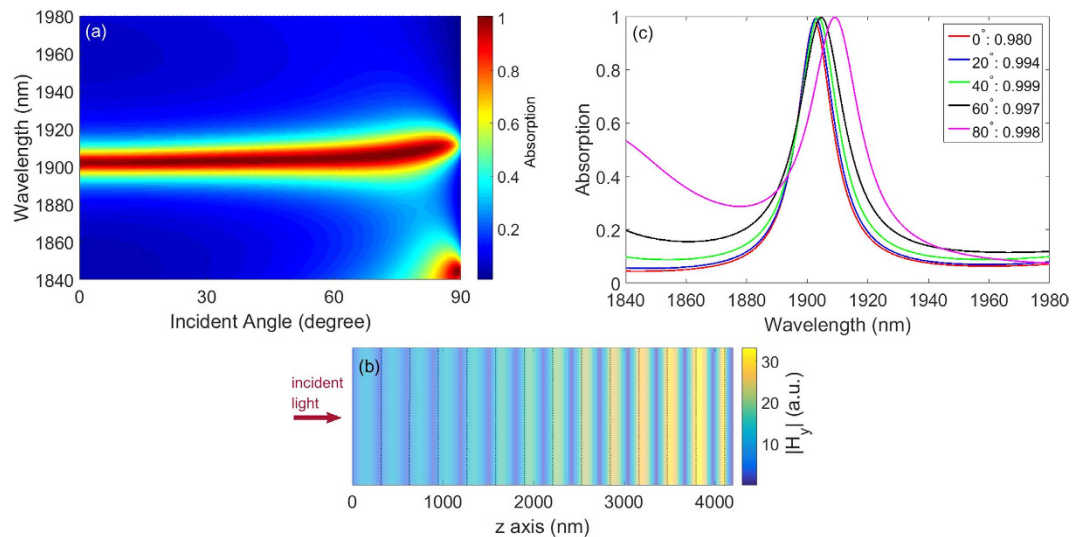


Figure 3. (a) The absorption spectra of the structure $((CD)_s B)_N$ on metal substrate for all angles of incidence. A flat and narrow-band absorption appears in the vicinity of 1902 nm. (b) The magnetic field distributions of the structure at 1902 nm for normal incidence. The dotted line indicates the interface between unit cell of 1DPC. (c) The absorption spectra of the structure at representative angles of incidence. The labels for the curves show the angles of incidence and the value of corresponding absorption peak.

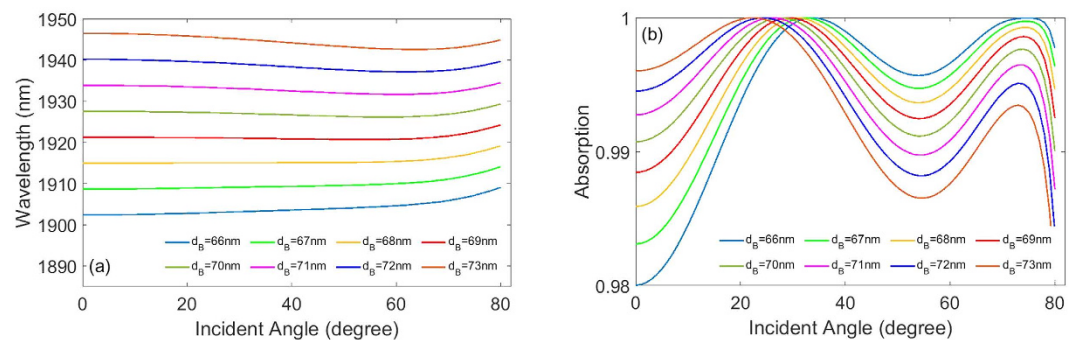


Figure 4. (a) The dependence of wavelength of absorption peak on angle of incidence at different thickness d_B . (b) The dependence of value of absorption peak on angle of incidence at different thickness d_B .

In order to reveal the narrow-band and wide-angle absorption properties of TPPs clearly, we illustrate the absorption spectra of structure at representative angle of incidence in Fig. 3(c). On the one hand, the value of absorption peak is 0.98 for normal incidence. With an increase of θ , the value of absorption peak is always nearly 1, from 0.994 at 20 degree, to 0.998 at 80 degree. Therefore near perfect absorptions are exhibited for all angles of incidence. On the other hand, there is a slight wavelength shift with an increase of θ . The wavelength of absorption peak appears at 1902 nm for normal incidence, and at 1909 nm for 80 degree. The wavelength shift of absorption peak versus angle of incidence is just 7 nm. By contrast, the full width at half maximum (FWHM) of the absorption spectrum is 15 nm for normal incidence and 23 nm for 80 degree. FWHM of the absorption spectrum is much smaller than the wavelength of absorption peak, which exhibits a narrow-band absorption spectrum. Likewise, the wavelength shift of absorption peak is smaller than FWHM of the absorption spectrum, which exhibits wide angle near perfect absorption.

Moreover, our perfect absorber design is flexible for the structural parameters. The change of structural parameters does not essentially influence the performance of absorber. Here we change the thickness d_B and investigate the performance of absorption peak. Firstly, as mentioned above, the absorption peak shows a slight shift to long wavelengths (~ 7 nm) when $d_B = 66$ nm. If increasing the thickness d_B , shown in Fig. 4(a), the wavelength shift of absorption peak becomes more slightly. When $d_B = 69$ nm, The wavelength of absorption peak even is invariant in the angle of incidence region of 0~70 degree, despite of slight shift to long wavelengths (~ 2 nm) in the angle of incidence region of 70~80 degree. Therefore, an optimized wide angle absorption behavior is exhibited in the case of $d_B = 69$ nm. If further increasing the thickness d_B , the wavelength of absorption peak shifts to short wavelengths in the angle of incidence region of 0~70 degree, and then turns to long wavelengths in the angle of incidence region of 70~80 degree. However, the total wavelength shift of absorption peak is just 3 nm even if d_B increases to 73 nm. Anyway, the wavelength shift of absorption peak is still rather slightly. In addition, we can see

from Fig. 4(b) that the value of absorption peak is always more than 0.98 in the angle of incidence region of 0~80 degree for the considered region of thickness d_B .

Conclusion

In summary, we have illustrated a simple design of a multilayer, wide-angle absorber exhibiting spectrally selective near-unity absorption. Spectrally selective perfect absorber is a specific application which requires both narrow band and wide-angle EM response. On the one hand, TPPs existing on 1DPC-metal interface induce penetration of EM waves into metal substrate, and then EM waves are absorbed entirely by lossy metal. On the other hand, phase variation compensation effect existing in 1DPC containing HMMs provide the methods of tailoring reflection phase, which can be used for realizing wide-angle TPPs under TM polarization. As a result, when 1DPC containing HMMs is combined with metal substrate, a narrow-band and wide-angle perfect absorption based on resonant tunneling effect is realized. The value of absorption peak is over 98% in the angle of incidence region of 0~80 degree and its FWHM just is 23 nm. Moreover, the simplicity of the structure is beneficial to its fabrication. We believe that such spectrally selective perfect absorbers possess potential applications for sensitive detectors and narrow-band thermophotovoltaic emitters.

References

- Shelby, R. A., Smith, D. R. & Schultz, S. Experimental Verification of a Negative Index of Refraction. *Science* **292**, 77 (2001).
- Pendry, J. B. Negative Refraction Makes a Perfect Lens. *Phys. Rev. Lett.* **85**, 3966 (2000).
- Schurig, D. *et al.* Metamaterial Electromagnetic Cloak at Microwave Frequencies. *Science* **314**, 977 (2006).
- Landy, N. I., Sajuyigbe, S., Mock, J. J., Smith, D. R. & Padilla, W. J. Perfect Metamaterial Absorber. *Phys. Rev. Lett.* **100**, 207402 (2008).
- Wu, C., Neuner, B. III & Shvets, G. Large-area wide-angle spectrally selective plasmonic absorber. *Phys. Rev. B* **84**, 075102 (2011).
- Greffet, J.-J. *et al.* Coherent emission of light by thermal sources. *Nature* **416**, 61 (2002).
- Laroche, M., Carminati, R. & Greffet, J.-J. Near-field thermophotovoltaic energy conversion. *J. Appl. Phys.* **100**, 063704 (2006).
- Nefzaoui, E., Drevillon, J. & Joulain, K. Selective emitters design and optimization for thermophotovoltaic applications. *J. Appl. Phys.* **111**, 084316 (2012).
- Teperik, T. V. *et al.* Omnidirectional absorption in nanostructured metal surfaces. *Nature Photonics* **2**, 299 (2008).
- Thongrattanasiri, S., Koppens, F. H. L. & García de Abajo, F. J. Complete Optical Absorption in Periodically Patterned Graphene. *Phys. Rev. Lett.* **108**, 047401 (2012).
- Hao, F., Nordlander, P., Sonnefraud, Y., Van Dorpe, P. & Maier, S. A. Tunability of subradiant dipolar and fano-type plasmon resonances in metallic ring/disk cavities: implications for nanoscale optical sensing. *ACS Nano* **3**, 643 (2009).
- Liu, N., Mesch, M., Weiss, T., Hentschel, M. & Giessen, H. Infrared perfect absorber and its application as plasmonic sensor. *Nano Lett.* **10**, 2342 (2010).
- Kabashin, A. V. *et al.* Plasmonic nanorod metamaterials for biosensing. *Nature Mater.* **8**, 867 (2009).
- Diem, M., Koschny, T. & Soukoulis, C. M. Wide-angle perfect absorber/thermal emitter in the terahertz regime. *Phys. Rev. B* **79**, 033101 (2009).
- Hao, J. *et al.* High performance optical absorber based on a plasmonic metamaterial. *Appl. Phys. Lett.* **96**, 251104 (2010).
- Fang, Z., Zhen, Y.-R., Fan, L., Zhu, X. & Nordlander, P. Tunable wide-angle plasmonic perfect absorber at visible frequencies. *Phys. Rev. B* **85**, 245401 (2012).
- Kaliteevski, M. *et al.* Tamm plasmon-polaritons: Possible electromagnetic states at the interface of a metal and a dielectric Bragg mirror. *Phys. Rev. B* **76**, 165415 (2007).
- Sasin, M. E. *et al.* Tamm plasmon polaritons: Slow and spatially compact light. *Appl. Phys. Lett.* **92**, 251112 (2008).
- Zhang W. L. & Yu, S. F. Opt. Commun. *Bistable switching using an optical Tamm cavity with a Kerr medium* **283**, 2622 (2010).
- Xue, C. H., Jiang, H. T. & Chen, H. Highly efficient all-optical diode action based on light-tunneling heterostructures. *Opt. Express* **18**, 7479 (2010).
- Afinogenov, B. I., Bessonov, V. O. & Fedyanin, A. A. Second-harmonic generation enhancement in the presence of Tamm plasmon-polaritons. *Opt. Lett.* **39**, 6895 (2014).
- Xue, C. H., Jiang, H. T., Lu, H., Du, G. Q. & Chen, H. Efficient third-harmonic generation based on Tamm plasmon polaritons. *Opt. Lett.* **38**, 959 (2013).
- Symonds, C. *et al.* Lasing in a hybrid GaAs/silver Tamm structure. *Appl. Phys. Lett.* **100**, 121122 (2012).
- Gazzano, O. *et al.* Single photon source using confined Tamm plasmon modes. *Appl. Phys. Lett.* **100**, 232111 (2012).
- Xue, C. H. *et al.* Dispersionless gaps and cavity modes in photonic crystals containing hyperbolic metamaterials. *Phys. Rev. B* **93**, 125310 (2016).
- Smith, D. R. & Schurig, D. Electromagnetic wave propagation in media with indefinite permittivity and permeability tensors. *Phys. Rev. Lett.* **90**, 077405 (2003).
- Poddubny, A., Iorsh, I., Belov, P. & Kivshar, Y. Hyperbolic metamaterials. *Nature Photon.* **7**, 958 (2013).
- Ferrari, L., Wu, C., Lepage, D., Zhang, X. & Liu, Z. W. Hyperbolic metamaterials and their applications. *Prog. Quantum Electron.* **40**, 1 (2015).
- Liu, Z., Lee, H., Xiong, Y., Sun, C. & Zhang, X. Far-field optical hyperlens magnifying sub-diffraction-limited objects. *Science* **315**, 1686 (2007).
- Yao, J., Yang, X., Yin, X., Bartal, G. & Zhang, X. Three-dimensional nanometer-scale optical cavities of indefinite medium. *Proc. Natl. Acad. Sci.* **108**, 11327 (2011).
- Jacob, Z., Smolyaninov, I. I. & Narimanov, E. E. Broadband purcell effect: radiative decay engineering with metamaterials. *Appl. Phys. Lett.* **100**, 181105 (2012).
- Iorsh, I., Poddubny, A., Orlov, A., Belov, P. & Kivshar, Y. S. Spontaneous emission enhancement in metal-dielectric metamaterials. *Phys. Lett. A* **376**, 185 (2012).
- Poddubny, A. N., Belov, P. A. & Kivshar, Y. S. Spontaneous radiation of a finite-size dipole emitter in hyperbolic media. *Phys. Rev. A* **84**, 023807 (2011).
- Potemkin, A. S., Poddubny, A. N., Belov, P. A. & Kivshar, Y. S. Green function for hyperbolic media. *Phys. Rev. A* **86**, 023848 (2012).
- Poddubny, A. N., Belov, P. A. & Kivshar, Y. S. Purcell effect in wire metamaterials. *Phys. Rev. B* **87**, 035136 (2013).
- Guo, Y., Cortes, C. L., Molesky, S. & Jacob, Z. Broadband super-Planckian thermal emission from hyperbolic metamaterials. *Appl. Phys. Lett.* **101**, 131106 (2012).
- Biehs, S.-A., Tschikin, M. & Ben-Abdallah, P. Hyperbolic metamaterials as an analog of a blackbody in the near field. *Phys. Rev. Lett.* **109**, 104301 (2012).
- Nefedov, I. S. & Simovski, C. R. Giant radiation heat transfer through micron gaps. *Phys. Rev. B* **84**, 195459 (2011).
- Krishnamoorthy, H. N. S., Jacob, Z., Narimanov, E., Kretzschmar, I. & Menon, V. M. Topological transitions in metamaterials. *Science* **336**, 205 (2012).

40. Shen, H. *et al.* Anomalously weak scattering in metal-semiconductor multilayer hyperbolic metamaterials. *Phys. Rev. X* **5**, 021021 (2015).
41. Saha, B. *et al.* TiN/(Al, Sc)N metal/dielectric superlattices and multilayers as hyperbolic metamaterials in the visible spectral range. *Phys. Rev. B* **90**, 125420 (2014).
42. Palik, E. D. *Handbook of Optical Constants of Solids I* (Academic Press, 1985).
43. West, P. R. *et al.* Searching for better plasmonic materials. *Laser Photonics Rev.* **4**, 795 (2010).
44. Gerfin, T. & Gratzel, M., Optical properties of tin-doped indium oxide determined by spectroscopic ellipsometry. *J. Appl. Phys.* **79**, 1722 (1996).
45. Jiang, H. T. *et al.* Enhancement of optical effects in zero-reflection metal slabs based on light-tunneling mechanism in metamaterials. *AIP Advances* **2**, 041412 (2012).

Acknowledgements

This work was financially supported by the National Key Research Program of China (No. 2016YFA0301101), by the National Natural Science Foundation of China (No. 11264003, No. 61661007, No. 61661007, No. 11234010, No. 11474220 and No. 11404102), by the Guangxi Natural Science Foundation (No. 2016GXNSFAA380198), and by the project of outstanding young teachers' training in higher education institutions of Guangxi.

Author Contributions

C.-H.X. carried out most of the simulation work and drafted most of the manuscript. F.W. carried out part of the simulation work and drafted part of the manuscript. H.-T.J. and Y.L. gave valuable discussions and contributed to the manuscript preparation. Y.-W.Z. and H.C. supervised the whole work. All authors reviewed the manuscript.

Additional Information

Competing financial interests: The authors declare no competing financial interests.

How to cite this article: Xue, C.-h *et al.* Wide-angle Spectrally Selective Perfect Absorber by Utilizing Dispersionless Tamm Plasmon Polaritons. *Sci. Rep.* **6**, 39418; doi: 10.1038/srep39418 (2016).

Publisher's note: Springer Nature remains neutral with regard to jurisdictional claims in published maps and institutional affiliations.



This work is licensed under a Creative Commons Attribution 4.0 International License. The images or other third party material in this article are included in the article's Creative Commons license, unless indicated otherwise in the credit line; if the material is not included under the Creative Commons license, users will need to obtain permission from the license holder to reproduce the material. To view a copy of this license, visit <http://creativecommons.org/licenses/by/4.0/>

© The Author(s) 2016